

in Figure 2. The characteristics of this PV cell can be obtained using standard equation (1).

$$I = I_{PV} - I_0 \left[\exp\left(\frac{V+R_S I}{V_t a}\right) - 1 \right] - \frac{V+R_S I}{R_p} \quad (1)$$

I_{PV} = photovoltaic current

I_0 = saturation current

V_t = $N_s k T/q$, thermal voltage of array

N_s = cell connected in series

T = is the temperature of the p-n junction

k = Boltzmann constant

q = electron charge

R_S = equivalent series resistance of the array

R_p = equivalent parallel resistance of the array

a = diode ideality constant

Figure 2 shows the single diode model. A single solar cell will produce only a limited power. Therefore it is usual practice in order to get desired power rating the solar cells are connected in parallel and series circuits which form a module. Such modules are again connected in parallel and series to form a solar array or panel to get required voltage and current. The equivalent series and parallel resistance of the array are denoted by the symbol R_S and R_p respectively in the equivalent circuit.

From the general I - V characteristic of the practical photovoltaic device one can observe that the series resistance R_S value will dominate in the voltage source region and the parallel resistance R_p value will dominate in the current source region of operation.

The general equation of a PV cell describes the relationship between current and voltage of the cell. Since the value of shunt resistance R_p is high compared to value of series resistance R_S the current through the parallel resistance can be neglected. The light generated current of the photovoltaic cell depends linearly on the solar irradiation and is also influenced by the temperature [9] given by the equation (2)

$$I_{PV} = [I_{PV,n} + K_I \Delta T] \frac{G}{G_n} \quad (2)$$

$I_{PV,n}$ = is the light generated current at nominal condition (25°C and 1000 W/m^2)

ΔT = $T - T_n$

T = actual temperature [K]

T_n = nominal temperature [K]

K_I = current coefficients

G = irradiation on the device surface [W/m^2]

G_n = nominal irradiation

$$I_0 = \frac{I_{sc,n} + K_I \Delta T}{\exp\left(\frac{V_{oc,n} + K_V \Delta T}{a V_t}\right) - 1} \quad (3)$$

K_V = voltage coefficients

K_I = current coefficients

The current and voltage coefficients K_V and K_I are included as shown in equation (3) in order to take the saturation current I_0 which is strongly dependent on the temperature.

The output voltage is increased (where the current remain unchanged) proportionally on number of identical PV modules connected in series (N_{ser}). Similarly the output current is increased (where the voltage remain unchanged) proportionally on number of identical PV modules connected

in parallel (N_{par}). It can be noted that the equivalent series and parallel resistance are directly proportional to the number of series modules and inversely proportional to the number of parallel modules respectively. The equation for array composed of $N_{ser} \times N_{par}$ given by equation (4)

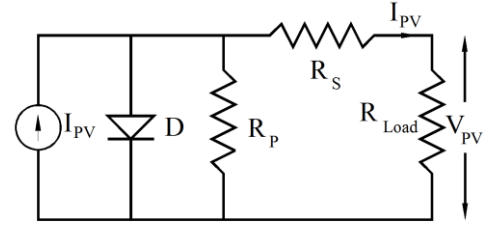


Figure 2: Equivalent circuit of PV cell

$$I = I_{PV} N_{par} - I_0 N_{par} \left[\exp\left(\frac{V + R_S \left(\frac{N_{ser}}{N_{par}}\right) I}{V_t a N_{ser}}\right) - 1 \right] - \frac{V + R_S \left(\frac{N_{ser}}{N_{par}}\right) I}{R_p \left(\frac{N_{ser}}{N_{par}}\right)} \quad (4)$$

I_{mp}	4.40 A	V_{oc}	21.20 V
V_{mp}	17.00 V	a	1.3
P_{max}	74.8 W	R_{se}	0.511 Ω
I_{sc}	5.02 A	R_{sh}	44.25 Ω
N_s	36	K_v	-74.7 mV/ $^\circ\text{C}$
$I_{0,n}$	9.83×10^{-8} A	K_I	2.80 mA/ $^\circ\text{C}$

Table I. Parameter of KCP -12075 solar array at 25°C , 1000 W/m^2

The parameter of solar array (KCP -12075 at 25°C , 1000 W/m^2) used for theoretical and experimental setup is given in table I.

III. DYNAMIC MODELING OF SESPIG

The d-q representation of single-phase two-winding induction generator is shown in Figure 3.

The dynamic equations [10] governing the stator and the rotor currents in the stator flux coordinates can be written as follows

$$(L_{lds}) \frac{d}{dt} (i_{ds}) = v_{ds} - r_{ds} i_{ds} - \frac{d}{dt} (\Psi_{md}) \quad (5)$$

$$(L_{lqs} + L_L) \frac{d}{dt} (i_{qs}) = v_{qs} - r_{qs} i_{qs} - R_L i_{qs} - \frac{d}{dt} (\Psi_{mq}) \quad (6)$$

$$(L_{ldr}) \frac{d}{dt} (i_{dr}) = v_{dr} - r_{dr} i_{dr} - \frac{d}{dt} (\Psi_{md}) - a \omega_r (L_{lqr} i_{qr} + \Psi_{mq}) \quad (7)$$

$$(L_{lqr}) \frac{d}{dt} (i_{qr}) = v_{qr} - r_{qr} i_{qr} - \frac{d}{dt} (\Psi_{mq}) + \frac{\omega_r}{a} (L_{ldr} i_{dr} + \Psi_{md}) \quad (8)$$

The state equations of capacitor bank are derived using the d-q components of stator voltages as state variables from the Figure 3.

$$\frac{d}{dt} (v_{ds}) = -\frac{i_{ds}}{C_{sh}} \quad (9)$$

$$\frac{d}{dt} (v_{qs}) = -\frac{i_{qs}}{C_{se}} \quad (10)$$

where

$$\Psi_{mq} = L_{mq} i_{mq} \Psi_{md} = L_{md} i_{md}$$

$$i_{mq} = i_{qs} + i_{qr} i_{md} = i_{ds} + i_{dr}$$

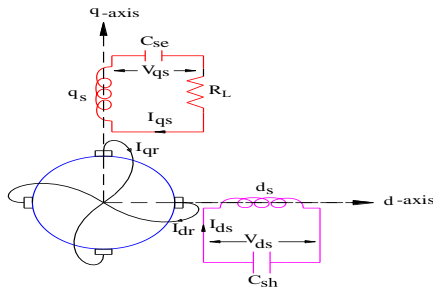


Figure 3: Circuit representation of the single-phase in d-q axes stationary reference frame

IV. STEADY STATE MODELING OF SESPIG

The steady-state equivalent circuit of SESPIG is shown in Figure 4.

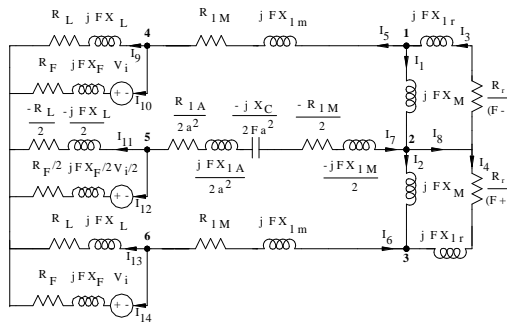


Figure 4: Equivalent circuit of SESPIG

The parameters of equivalent circuit are:

$$\begin{aligned} Z_1 &= jFX_M; \\ Z_2 &= Z_1; \\ Z_3 &= R_2 \dot{F}/(F - u) + jFX_{1r}; \\ Z_4 &= R_2 \dot{F}/(F + u) + jFX_{1r}; \\ Z_5 &= R_{1M} + jFX_{1M}; \\ Z_6 &= Z_5; \\ Z_7 &= R_{1A}/2a^2 + jFX_{1A}/2a^2 - jXC/2Fa^2 - R_{1M}/2 - jFX_{1M}/2; \\ Z_L &= R_L + jFX_L \end{aligned}$$

$$\begin{bmatrix} (Y_1 + Y_3 + Y_5) & -(Y_1 + Y_3) & 0 & -(Y_5) & 0 & 0 \\ -(Y_1 + Y_3) & (Y_1 + Y_2 + Y_3 + Y_4 + Y_7) & -(Y_2 + Y_4) & 0 & -(Y_7) & 0 \\ 0 & -(Y_2 + Y_4) & (Y_6 + Y_2 + Y_4) & 0 & 0 & -(Y_6) \\ -(Y_5) & 0 & 0 & (Y_5 + Y_L + Y_i) & 0 & 0 \\ 0 & -(Y_7) & 0 & 0 & (Y_7 + Y_L + Y_{i1}) & 0 \\ 0 & 0 & -(Y_6) & 0 & 0 & (Y_6 + Y_L + Y_{i1}) \end{bmatrix} \begin{bmatrix} V_1 \\ V_2 \\ V_3 \\ V_4 \\ V_5 \\ V_6 \end{bmatrix} = \begin{bmatrix} 0 \\ 0 \\ 0 \\ -V_i/Z_i \\ -V_i/Z_i \\ -V_i/Z_i \end{bmatrix} \quad (13)$$

The matrix (13) is formed from the per-phase equivalent circuit is shown in Figure 4. The terminal voltage and the frequency of the induction machine are fixed at the nominal level [11]. The matrix (13) can be inverted to find the node voltages V_1, V_2, V_3, V_4, V_5 and V_6 respectively. Once the node voltages are found the inverter current from equation (12) can be obtained for a given speed and inverter voltages V_i . The value of magnetizing reactance X_M is calculated from the magnetization characteristics. The parameters of the laboratory machine along with magnetization characteristics

$$Z_{LT} = Z_L$$

$$Z_{L1} = -R_L/2 - jFX_L/2$$

$$Z_{iT} = R_F + jFX_F + V_i$$

$$Z_i = Z_{iT}$$

$$Z_{i1} = R_F/2 + jFX_F/2 + V_i/2$$

The branch admittances are:

$$Y_1 = 1/Z_1; \quad Y_2 = 1/Z_2; \quad Y_3 = 1/Z_3;$$

$$Y_4 = 1/Z_4; \quad Y_5 = 1/Z_5; \quad Y_6 = 1/Z_6;$$

$$Y_7 = 1/Z_7; \quad Y_L = 1/Z_L; \quad Y_{LT} = 1/Z_{LT};$$

$$Y_{L1} = 1/Z_{L1}; \quad Y_{iT} = 1/Z_{iT}; \quad Y_i = 1/Z_i;$$

$$Y_{i1} = 1/Z_{i1}$$

Let V_1, V_2, V_3, V_4, V_5 and V_6 be the node voltages at nodes 1, 2, 3, 4, 5 and 6 respectively. By applying Kirchoff's current law at nodes 1, 2, 3, 4, 5 and 6 respectively the following equations (11) can be obtained.

$$I_3 = I_1 + I_5$$

$$I_1 = I_2 + I_3 + I_4 + I_7$$

$$I_6 = I_2 + I_4$$

$$I_5 = I_8 + I_9$$

$$I_7 = I_{10} + I_{11}$$

$$I_6 = I_{12} + I_{13} \quad (11)$$

where,

$$I_1 = (V_1 - V_2)Y_1; \quad I_2 = (V_2 - V_3)Y_2;$$

$$I_3 = (V_2 - V_1)Y_3; \quad I_4 = (V_2 - V_3)Y_4;$$

$$I_5 = (V_1 - V_4)Y_5; \quad I_6 = (V_3 - V_6)Y_6;$$

$$I_7 = (V_2 - V_5)Y_7; \quad I_8 = (V_4 + V_i)Y_{iT};$$

$$I_9 = V_4 Y_{LT}; \quad I_{10} = (V_5 + V_i/2)Y_{i1}/2$$

$$I_{11} = (V_5)Y_{L1}/2; \quad I_{12} = (V_6 + V_i)Y_i;$$

$$I_{13} = V_6 Y_L; \quad (12)$$

On substituting equations (12) in equations (11) and rearranging the resulting equations in matrix form, we can get the following matrix

of the test system and the flowchart for predicting the steady-state response are given in the Appendix.

V. DC-DC BOOST CONVERTER

A dual stage power electronic system comprising a boost type dc-dc converter and an inverter is used to feed the power generated by the PV array to the load. To maintain the load voltage constant a DC-DC step up converter is introduced between the PV array and the inverter. The block schematic

of the proposed scheme is shown in Figure 1. In this scheme a PV array feeds DC-DC converter used in step-up configuration. The voltage across the DC-DC converter is fed to a single-phase, quasi-square-wave IGBT inverter a single-phase fixed amplitude and fixed frequency supply is obtained to feed an isolated load. For a dc-dc boost converter, by using the averaging concept, the input-output voltage relationship for continuous conduction mode is given by

$$V_o/V_{in} = 1/(1 - D) \tag{21}$$

Where, D = duty cycle. Since the duty ratio “D” is between 0 and 1 the output voltage must be higher than the input voltage in magnitude. It should be noted that the control logic of such dc-dc converter has to be different when it is fed from a stiff DC source. The duty ratio of the chopper is found to increase linearly with increase in cell temperature and hence the intensity.

As the inverter DC voltage varies with irradiation to obtain constant amplitude and constant frequency supply from the inverter, a closed loop fuzzy controller is incorporated to automatically vary the duty-cycle of the DC-DC converter to obtain constant DC voltage at the inverter input terminals. The inverter output is then applied to an isolated load. At the same time fuzzy controller will maintain the output voltage of inverter by supplying the required reactive power according to the change in speed of the wind and load. This can be achieved by maintaining the battery voltage adequately high.

VI. FUZZY LOGIC MPPT CONTROLLERS

The conventional PI controllers are fixed-gain feedback controllers. Therefore they cannot compensate the parameter variations in the process and cannot adapt changes in the environment. PI-controlled system is less responsive to real and relatively fast alterations in state and so the system will be slower to reach the set point. On the other hand P&O method for MPPT tracking will not respond quickly to rapid changes in temperature or irradiance. Therefore the fuzzy control algorithm is capable of improving the tracking performance as compared with the classical methods for both linear and nonlinear loads. Also, fuzzy logic is appropriate for nonlinear control because it does not use complex mathematical equation.

The two FLC input variables are the error E and change of error ΔE. The behavior of a FLC depends on the shape of membership functions of the rule base. In this paper a fuzzy logic control scheme (Figure 1) is proposed for maximum solar power tracking of the PV array with an inverter for supplying isolated loads. They have advantages to be robust and relatively simple to design since they do not require the knowledge of the exact model. On the other hand the designer needs complete knowledge of the hybrid system operation.

A. Fuzzification

The membership function values are assigned to the linguistic variables using seven fuzzy subset called negative

big (nb), negative medium (nm), negative small (ns), zero(zr), positive small (ps), positive medium (pm), positive big (pb). Fuzzy associative memory for the proposed system is given in Table-2. Variable e and Δe are selected as the input variables, where e is the error between the reference voltage (V_r) and actual voltage (V_o) of the system, Δe is the change in error in the sampling interval. The output variable is the reference signal for PWM generator U. Triangular membership functions are selected for all these process. The range of each membership function is decided by the previous knowledge of the proposed scheme parameters.

B. Inference engine

Inference engine mainly consist of Fuzzy rule base and fuzzy implication sub blocks. The inputs are now fuzzified are fed to the inference engine and the rule base is then applied. The output fuzzy set are then identified using fuzzy implication method. Here we are using MIN-MAX fuzzy implication method.

C. Defuzzification

Once fuzzification is over, output fuzzy range is located. Since at this stage a non-fuzzy value of control is available a defuzzification stage is needed. Centroid defuzzification method [12] is used for defuzzification in the proposed

Table2. Fuzzy associative memory for the proposed system

e	Δe						
	nb	nm	ns	zr	ps	pm	pb
nb	nb	nb	nb	nm	nm	ns	zr
nm	nb	nb	nm	nm	ns	zr	ps
ns	nb	nm	nm	ns	zr	ps	pm
zr	nm	nm	ns	zr	ps	pm	pm
ps	nm	ns	zr	ps	pm	pm	pb
pm	ns	zr	ps	pm	pm	pb	pb
pb	zr	ps	pm	pm	pb	pb	pb

scheme. The membership function of the variables error, change in error and change in reference signal for PWM generator are given in Table 2.

VII. RESULTS AND DISCUSSION

A MATLAB based modeling and simulation scheme (Appendix) with fuzzy logic controller is proposed which are suitable for studying performance of the hybrid scheme (Figure1). The photovoltaic I-V and P-V characteristics are discussed. Also, the steady-state and dynamic characteristics of the hybrid scheme under varying speed and load conditions are discussed.

A. PV-Characteristics

The behaviour the PV cells and its characteristics are discussed in this section. It is found that the set of P-V and I-V characteristics are highly nonlinear and dependent on solar irradiance of the PV array. Figure 5(a) and 5(b) shows P-V and I-V characteristics of a PV cell. It can be observed that as the cell temperature remain constant the PV output voltage remains nearly constant while the PV output current increases with increasing solar intensity.

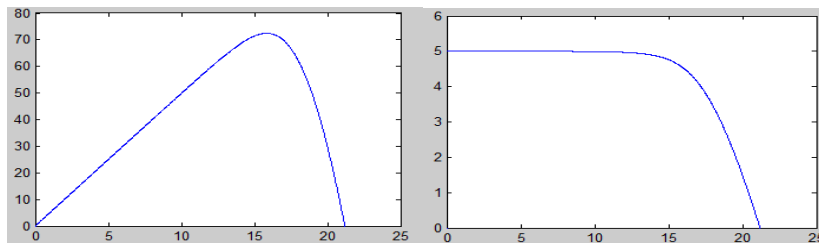


Figure5(a): P-V Characteristics

Figure5(b): I-V Characteristics

VIII. DYNAMIC RESPONSE OF HYBRID SCHEME

The simulated per phase current and voltage waveform across the load is shown in Figure6(a). The simulated per phase current waveform (Fig. 6(b)) shows, even though the load is applied at 2.25 seconds the voltage across the load

remains almost constant. Figure 6(c) and 6(d) shows the experimental waveforms of voltage and current respectively under loading conditions. Some harmonics have been introduced in the proposed scheme found in the waveforms it can be eliminated by introducing necessary filters.

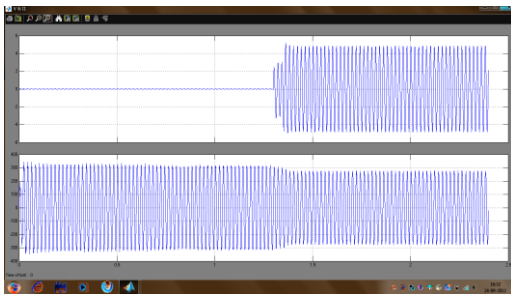


Figure 6(a).

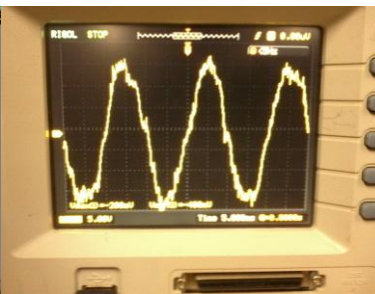


Figure 6(c).

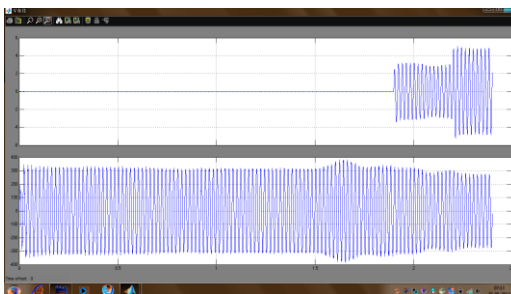


Figure 6(b).

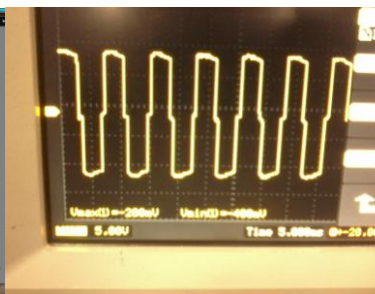


Figure 6(d).

Figure 6. Simulated and Experimental waveforms

IX. STEADY STATE PERFORMANCE OF HYBRID SCHEME

The per-phase equivalent circuit is shown in Figure. 4. A new mathematical model for the steady-state analysis in matrix form (equation 13) is presented in section IV. The steady state model includes the equivalent circuit of the inverter and its impedance of the inverter side filter. The steady-state characteristics under varying rotor speed of the SEIG from 1400 to 1700 rpm and minimum to maximum irradiation from 0.3 to 0.9 kW/m² of the PV cell are discussed.

Figure 7(a) shows wind speed variation from 1400 to 1700 rpm at minimum solar irradiation of 0.3kW/m². When the wind speed is around 1400 rpm (below synchronous speed) the PV array power increases (by proportionally varying the duty cycle of DC-DC converter) and supplies the additional power to the load through the inverter and hence the load voltage is maintained as desired. On the other hand when the wind speed is around 1550 rpm (above synchronous speed) the SEIG will supply directly the additional power to the load

and hence the load voltage is maintained as desired wherein the PV array power decreases.

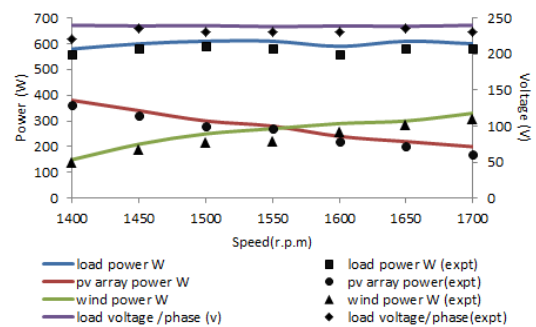


Figure. 7(a) Minimum irradiation and varying windspeed

Figure 7(b) shows wind speed variation from 1400 to 1700 rpm at maximum solar irradiation of 0.9kW/m². When the wind speed is around 1400 rpm (below synchronous speed) since the solar irradiation is maximum the PV array power

increases and supplies the additional power to the load through the inverter and hence the load voltage is maintained

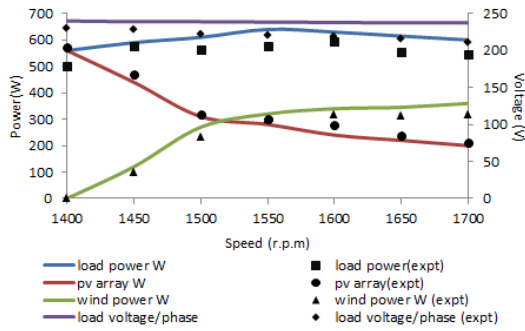


Figure. 7(b) Maximum irradiation and varying windspeed

as desired. On the other hand when the wind speed is around 1550 rpm (above synchronous speed) the SEIG will supply directly the additional power to the load and hence the load voltage is maintained as desired wherein the PV array power decreases (by proportionally varying the duty cycle of DC-DC converter).

Figure 7(c) shows variation of solar irradiation from 0.3 to

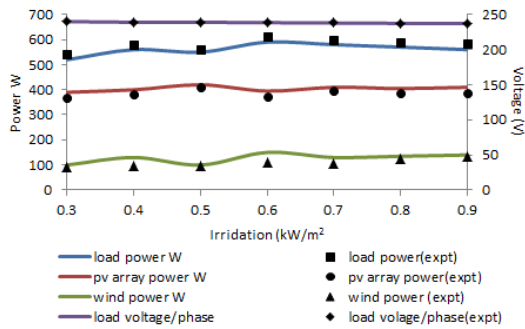


Figure. 7(c) Minimum wind speed and varying irradiation

0.9kW/m² at minimum wind speed of 1400rpm. When the irradiation is minimum of 0.3kW/m² the PV array power has to be increased by proportionally varying the duty cycle of DC-DC converter. Thus the additional power will be supplied by the PV array through the inverter to the load and hence the load voltage is maintained as desired. On the other hand when the irradiation is maximum of 0.9kW/m² the PV array power directly supplies the additional power to the load and hence the load voltage is maintained as desired.

Figure 7(d) shows variation of solar irradiation from 0.3 to

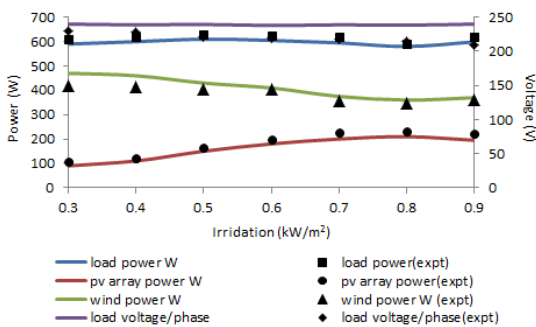


Figure. 7(d) Maximum wind speed and varying irradiation

0.9kW/m² at maximum wind speed of 1700rpm. When the irradiation is minimum of 0.3kW/m² the SEIG will directly supplies the additional power to the load and hence the load

voltage is maintained as desired. On the other hand when the irradiation is maximum of 0.9kW/m² the PV array power has to decreased by proportionally varying the duty cycle of DC-DC converter the SEIG still supplies the additional power to the load and hence the load voltage is maintained as desired.

The above said can be achieved by the proposed fuzzy logic controller which varies the duty cycle of DC-DC step up converter automatically. This proves the self-regulating mechanism of the proposed scheme.

X. CONCLUSION

A hybrid scheme for isolated application employing solar and single phase wind driven induction generator is proposed with fuzzy logic controller with optimized rule-base. A DC-DC converter is intervened between the PV array and the inverter to obtain constant load voltage with variations in irradiation and wind speed. Using the mathematical model described the photo-voltaic, dynamic and steady-state characteristics are discussed. The simulated and experimental waveforms are focused on both the steady-state and dynamic behaviour which demonstrate the validity of the proposed model. The experimental result of hybrid scheme shows the operation of the controller for constant load voltage had inherently resulted in balancing of power between the two sources while supplying constant power to the load.

APPENDIX

The flowchart for predicting the steady-state response discussed in section IV is given in Figure 8.

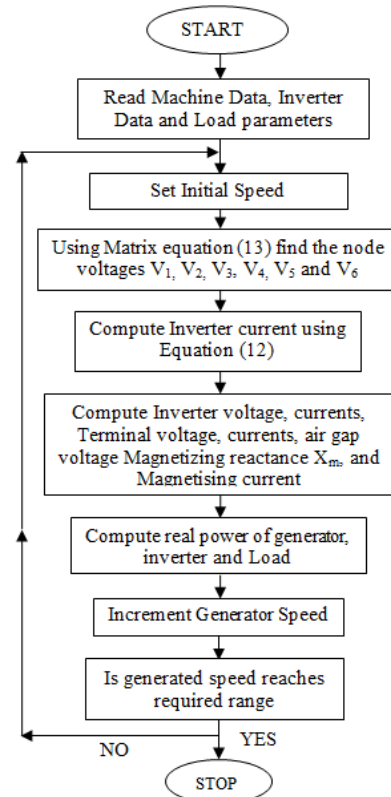


Figure 8. Flowchart for steady-state response

A MATLAB (version 7.9.0.529) based modeling and simulation scheme along with fuzzy logic controller is proposed (Figure9) which are suitable for studying the steady-state and dynamic behaviour of the hybrid system.

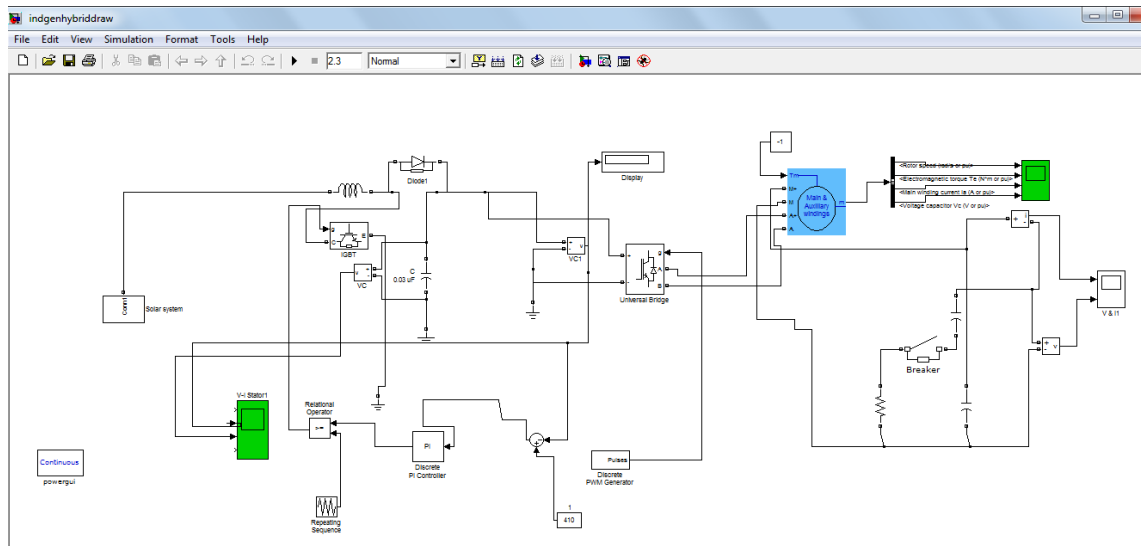


Figure 9. Hybrid solar/wind scheme with fuzzy controller in simulink (version 7.9.0.529)

Machine Parameters

Base values:

V_{base} = rated voltage	= 230 V
I_{base} = rated current	= 2 A
$Z_{base} = V_{base} / I_{base}$	= 38.33 ohms
Base power $P_{base} = V_{base} * I_{base}$	= 0.75 kW
Base speed N_{base}	= 1500 rpm
Base frequency f_{base}	= 50 Hz

The p.u parameters of the machine are:

$$R_{1M} = 0.0734, \quad R_2 = 0.1036, \quad X_{1M} = X_{1r} = 0.1675, \\ R_{1A} = 0.1357, \quad X_{1A} = 0.3074, \quad \text{and } a = 1.25$$

The magnetizing reactance X_M versus air gap voltage V_g/F expressed (in p.u) by a set of piecewise linear approximations are given below.

$$V_g/F = 1.689 - 0.2X_M \quad \text{for } X_M \leq 3.2 \\ V_g/F = 2.844 - 0.555X_M \quad \text{for } X_M > 3.2$$

ACKNOWLEDGMENT

The authors gratefully acknowledge the support and facilities provided by the authorities of Annamalai University, Annamalainagar, Tamilnadu, India to carry out this research work.

REFERENCES

- [1] S.Meenakshi, K.Rajambal, C.Chellamuthu, and S.Elangovan, "Intelligent Controller for Stand-Alone Hybrid Generation System", *Power India Conference IEEE*, pp 8-15, 2006.
- [2] Ashraf A.Ahmed, Li Ran, Jim Bumby, "Simulation and control of a Hybrid PV-Wind System", *Power Electronics Machines & Drives, PEMD 4th IET conference*, pp 421-425, 2008.
- [3] Meenakshmisundaram Arutchelvi, Samuel Arul Daniel, "Grid Connected Hybrid Dispersed Power Generators Based on PV Array And Wind Driven Induction Generator", *Journal of Electrical Engineering*, Vol., 60, pp 313-320, 2009.
- [4] T.Ahmed, N. Katsumi, N.Mutsuo, "Advanced control of PWM converter with variable-speed induction generator", *IET Electr.Power Appl*, pp 239-247, 2007.
- [5] S.Bhim, K.Gaurav kumar, "Solid state voltage and frequency controller for a stand- alone wind power generating system", *IEEE Trans.Power Electron*, pp 1170-1177, 2008.

- [6] B.Venkatesa perumal, K.Jayanta, "Voltage and frequency controller of a stand- alone brushless wind electric generation using generalized impedance controller" *IEEE Trans. Energy Convers*, pp 632-641, 2008.
- [7] S.Bhim, K.Gaurav kumar, "Voltage and frequency controller for three phase four wire autonomous wind energy conversion system", *IEEE Trans.Energy Convers*, pp 509-518, 2008.
- [8] M.G.Villalva, J.R.Gazol, and E.R.Filho, "Comprehensive Approach to Modeling and Simulation of Photovoltaic Arrays", *IEEE trans. on Power Electronics*, vol.24, no.5, pp.1198-1208, 2009.
- [9] H. Patel, and V. Agarwal, "MATLAB based modeling to study the effects of partial shading on PV array characteristics", *IEEE trans. on energy conv.*, vol. 23, no.1, pp. 302-310, 2008.
- [10] Bhim singh, L.B. Shilpakar, S.S Murthy, A.K. Tiwari, "Improved steady state and transient performance with optimum excitation of single phase self-excited induction generator", *Electric machines and power system*, 2000.
- [11] A.Karthikeyan, C.Nagamani, G.Saravana Illango, A.Sreenivasulu, "Hybrid, open-loop excitation system for a wind turbine -driven stand-alone induction generator", *IET Renewable Power Generation*, Vol.5, no.2, pp.184-193, 2011.
- [12] Timothy and Ross J, *Fuzzy logic with engineering applications*, McGraw hill international editions, Electrical engineering series, New York, 1997.